Evaluating Power Density for 5G Applications

Maryna Nesterova
Aprel Inc.
Kanata, Canada
MarynaN@aprel.com

Stuart Nicol
Aprel Inc.
Kanata, Canada
StuartN@aprel.com

Yuliya Nesterova
Queen's University
Kingston, Canada
9yn2@queensu.ca

***Abstract*—The next generation of wireless 5G technology is being continuously designed to meet the growing demand from different industries for more data, more devices, higher speed, and improved operational efficiency. While mmWave bands offer much higher bandwidths, they are subject to higher signal losses when compared to the lower frequency bands currently used for wireless technologies. As such, the industries involved require evolutionary methodologies for the thorough evaluation of 5G mobile devices. The authors offer an advanced near-field measurement technique as a solution for robust assessment of device performance. This novel method introduces the spatial vector evaluation of both electric E and magnetic H fields through the cross-detection of their interaction. Based in terms of the Poynting vector theorem, this two-probe technique provides a steady measurement-based orientation for research within the rapidly changing conditions of the mmWave environment.**

***Index Terms*—near-field measurement, 5G, E field, H field, phase shift, Poynting vector, power density, field patterns, beam-forming.**

I. Introduction

The specific feature of the near-field zone is non-synchronised E and H fields: on the resonating surface of an antenna the H-field oscillations are $\lambda/4$ shifted relative to the E-fields (Fig. 1a), whereas in the far-field zone the fluctuations of electric and magnetic fields are in phase (Fig. 1b), forming free-space signal propagation. The near-field zone is a transitional area characterised by the non-uniform field distributions for both E and H fields. As such, a signal phase is not well-defined in near field: the E and H magnitude oscillations are not coherent. The transition from non-synchronised E and H to the synchronised oscillations is a non-linear process and its complexity depends on the type of antenna and modulation type.

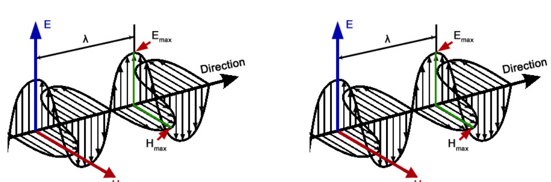

(a) Resonance (b) Propagation

Fig. 1. Electromagnetic Wave Propagation.

Although the field distribution variances for 5G antennas are substantial in close proximity to the device, the field flux orientation is constant within the region of the near-field zone: the shape of the field pattern changes from point to point (Fig. 2) and often is not symmetrical.

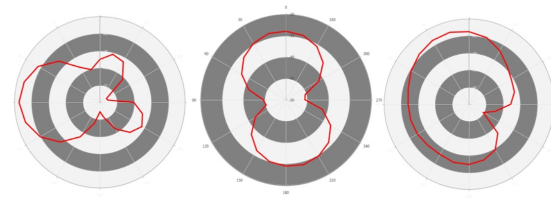

Fig. 2. Field patterns measured within different points of a scan grid.

To account for the anisotropy of the electromagnetic field in three-dimensional space, measurements on several spatial layers are essential for the comprehensive evaluation of the field distribution. This allows for the analysis of the complex fields as they begin to evolve and transition into free space.

II. Measurement procedure.

Assessment of 5G devices or complex broadband signals requires a new generation of instruments and measurement approaches. The signal beam of antennas operating at a frequency range from 20 GHz to 100 GHz is narrow, making testing in the far-field zone rather difficult. The key challenges are:

- narrow beam with an undefined orientation,
- high rate of signal decay over distance,
- complex modulations,
- high level of measurement uncertainty.

The authors propose a two-probe method, which is based on the well-defined methodology of measuring the electric E- and magnetic H- field magnitude in the reactive near-field zone. This novel approach for the evaluation of the field anisotropy allows for the correlation of these two fields through the Poynting vector theorem. Thus the power density, emitted power, and reverse field of energy can be quantified. These measurements are achieved using near field probes, which have been designed for the analysis of either the E or H vectors.

A. Measurement system

Aprel low Q antenna probes are designed and calibrated for cross detection, field directivity and field vector orientation. The 5G probes have been fully characterized and assessed for sensitivity in air from 6 GHz up to 110 GHz, including the effect of reactive near fields.

For the millimetre-wave antennas, an exceptional precision in probe positioning is essential, this is an imperative feature of the testing process. For such procedures, it is required that it be automated and controlled via a repeatable positioning system. The EM-ISight automated near-field measurement system (Fig. 3) provides a 0.02 mm positioning accuracy with a grid resolution of 0.05 mm. The E- or H- probe is attached to the Boundary Detection Unit (BDU) which is fixed on the robot arm and connected to either a vector network analyser or a real-time spectrum analyser.

Due to the geometry of the probe aperture, the scan can be performed at a close distance of 0.5 mm over the device surface. A boundary detection function allows for the antenna probe to be maintained for complex topologies (non-planar surfaces). During the test scan the antenna probe is rotated with a defined radial step dependent on the carrier frequency and complexity of the resonant structure (design).

B. Experiment Setup Description

The passive test sample operating at a frequency of 28 GHz was evaluated for both electric E and magnetic H field distributions.

For the presented study, the near-field E and H antenna probes were employed for measurements rotated every 15 degrees at each point within the scan grid. Antenna probes were rotated 360 degrees to evaluate the planar field distributions at a distance of 1mm from the surface of the device under test (further referred to as the DUT). The scan grid was 20 mm by 20 mm in X and Y directions.

The vector network or spectrum analyser settings depend on the carrier frequency and modulation bandwidth of the DUT. The measured spectral content for every point of a scan is recorded to the data file.

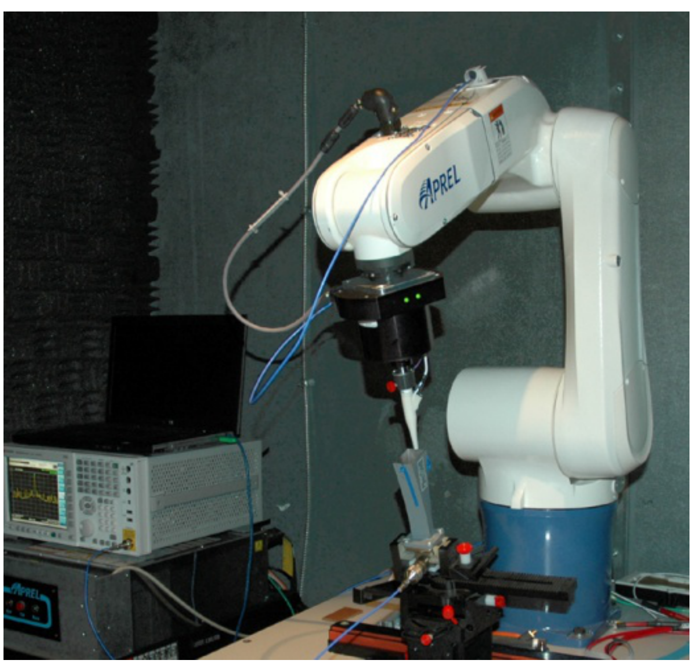

Fig. 3. Automatic system for near-field measurements.

C. Evaluation of Power Density in Near Field

As described in [1], in the reactive near-field zone electric and magnetic fields are not in phase, so the phase shift condition should be accounted for. This paper describes the need to account for the phase shift for both E and H in the reactive near-field. Fig. 4 represents the geometrical interpretation of the phase shift case. For the synchronised E and H fields, the angle between corresponding vectors is always 90 degrees and thus $\sin\theta$ equals 1. In the presence of a phase shift denoted by θ', the magnetic maximum amplitude vector is projected onto a perpendicular to the electric maximum amplitude vector. The details may be found in [2].

For this study a well-established technique for evaluation of the electromagnetic field power density has been used, based on the Poynting vector theorem [3], which presents power density $\vec{S}$ as a cross product of electric field $\vec{E}$ and magnetic field $\vec{B}$ vectors (1), where the field is presented in W/m^2.

$$\vec{S} = \frac{1}{\mu_0}\vec{E} \times \vec{B} \tag{1}$$

Using the formula (2), the Pointing vector equation can be presented in form (3):

$$B = \mu_0 H \tag{2}$$

$$\vec{S} = E \cdot H \sin(\theta)\,\hat{n} \tag{3}$$

where $\vec{S}$ is power density vector (W/m^2), E — the electric field amplitude (V/m), H — the magnetic field amplitude (A/m), θ — the angle between $\vec{E}$ and $\vec{B}$ vectors, $\hat{n}$ — the unit vector normal to both $\vec{E}$ and $\vec{B}$, B — the magnetic flux density (T), and μ_0 — the magnetic constant (H/m). Unless specified otherwise, the terms magnetic field and magnetic field vector are used to refer to H.

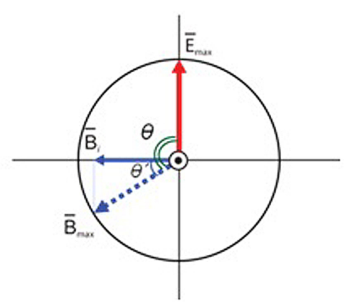

Fig. 4. Phase shift diagram.

Hence, the power density formula becomes:

$$S = E_{max} H_{max} \cos(\theta')\, n. \tag{4}$$

III. Test results

In the E and H field plots, each colour corresponds to the value of the maximum measured amplitude at every point of the grid and directional arrows indicate orientations of the field vectors (Fig. 5). Examination of the field currents exposed the smoothness of the E field generated by the antenna: vectors are oriented downwards along the Y axis on the left part of the plot, and upwards along the Y axis on the right side of the plot, both with ± 15-degree fluctuations. Conversely the H field current structure is more complicated and can be distinguished in clusters with different vector orientations.

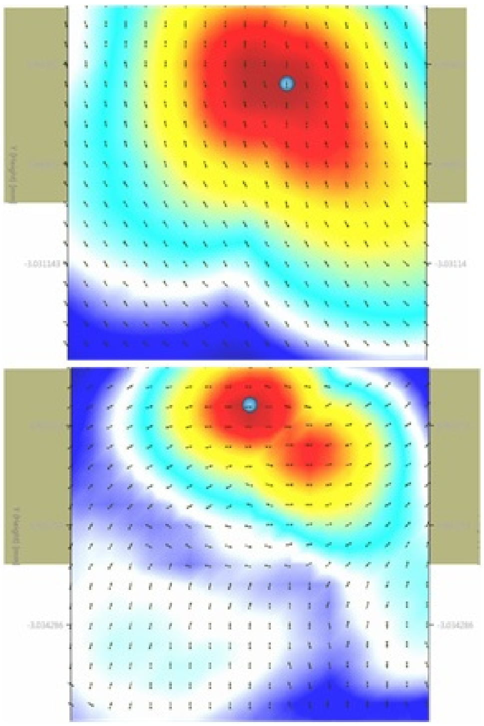

Fig. 5. Plots for E (top) and H (bottom) field vector distribution.

The polar charts in Fig. 6 present symmetrical and asymmetrical field patterns and maximum amplitude vector orientation for both cases. The locations of E and H peaks are different and the shapes of hotspots are diverse. These parameters, along with the angle between the maximum vectors of electric and magnetic fields, are forming the beam shape and its direction.

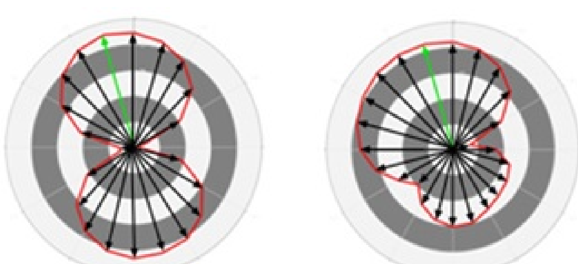

Fig. 6. Field patterns for different scan points. The maximum amplitude vector is highlighted.

IV. Data analysis

The RF-ISight analytical toolbox was used for data post-processing so as to calculate the power density. Because the two-probe method allows for complex and independent measurement of the angle between E and H fields, the scan results were processed for two types of power density:

- Isotropic (ISO) — uniform in all directions, and
- Directional (DIR) — accounting for the directional distribution of the E and H fields and the phase shift between them.

At each grid point within the scan grid the field distribution as a function of radial orientation was analysed to obtain the measured field maxima (Fig. 7: red vector) and averaged values (Fig. 7: green circle).

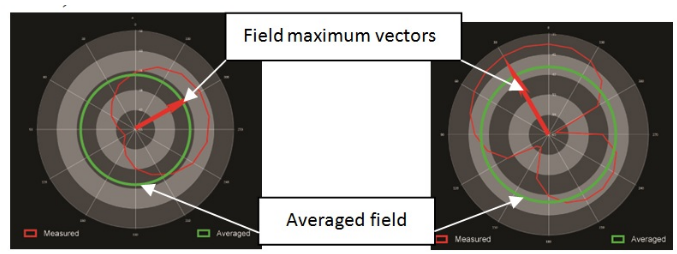

Fig. 7. Polar charts for a single point of the scan grid.

The distributions of isotropic fields (Fig. 8) differ in shape, value, and peak position from the directional data presented in Fig. 5. The Isotropic Peak represents the point of maximum average amplitude with small maximum-to-average ratio, whereas the Directional Peak indicates the vector of maximum amplitude measured.

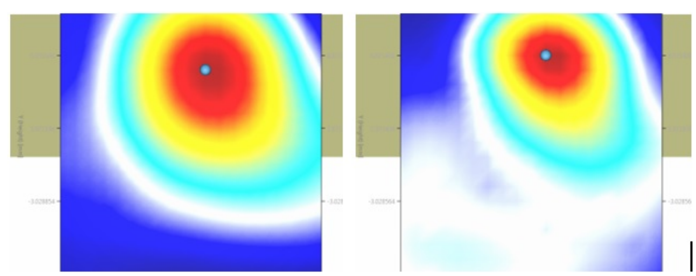

Fig. 8. sotropic E (left) and H (right) field distribution.

The isotropic power density is calculated without accounting for the angle between electric and magnetic vectors. There is a considerable difference between directional and isotropic power density plots (Fig. 9). The directional power density plot shows two lobes of propagating energy (red hotspots) and two narrow areas of back propagating power (navy blue areas).

The isotropic power density peak is about 50% lower than the directional peak, and the levels of averaged power over the areas of $1\ \mathrm{cm}^2$ and $4\ \mathrm{cm}^2$ are in the same proportion (Fig. 10).

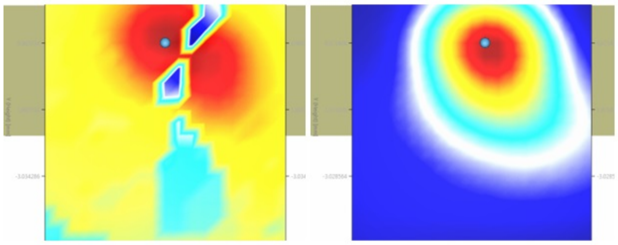

Fig. 9. Directional (left) and Isotropic power density plots.

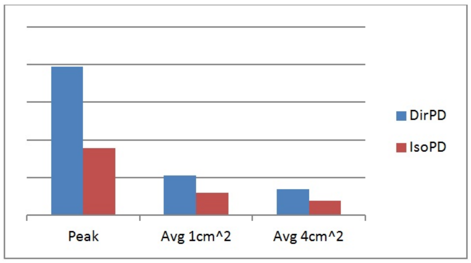

Fig. 10. Comparison diagram of Directional and Isotropic power density values: peak, averaged over $1\ \mathrm{cm}^2$ and over $4\ \mathrm{cm}^2$.

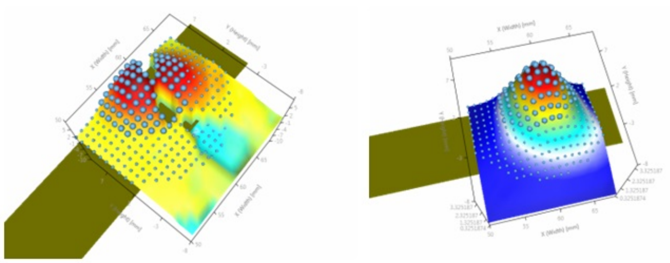

Fig. 11. Directional (left) and Isotropic power density 3D plots. Averaging area of $1\ \mathrm{cm}^2$ is covered by bigger spheres while $4\ \mathrm{cm}^2$ averaging area is covered by smaller dots.

The averaging areas for both types of power density are presented in Fig. 11. The comparison analysis for the averaged isotropic power density indicates that for the presented test case of 28 GHz the ratio between maximum and minimum values over the area of $1\ \mathrm{cm}^2$ is around 3dB and for $4\ \mathrm{cm}^2$ area — around 6dB.

Conclusions

The Pointing vector distribution provides comprehensive information for the robust assessment of antenna performance:

- Efficiency,
- Emitted power,
- Power density,
- Gain,
- Reverse propagation.

For the multi-layer test configuration additional parameters can be evaluated, such as:

- Direction of signal propagation,
- Beamforming (as described in [4]),
- Beam width angle,
- Energy dissipation rate over the $\frac{\lambda}{2}$, λ, and 2λ distance, (λ is wavelength).

The near-field test of the 5G antenna demonstrated that the two-probe method can be implemented on all stages of device development: from the optimization of antenna design to the MPE safety assessment.

References

[1] I. Straus, Near and far fields – from statics to radiation, Conformity, February 2001, www.conformity.com/0102reflections.html.

[2] M. Nesterova, S. Nicol, Y. Nesterova, Two-probe method for advanced EM wave propagation analysis, IEEE RADIO 2017 International Conference, September 2017.

[3] D. J. Griffiths, Introduction to Electrodynamics, Prentice-Hall, Inc., September 1999, pp. 347-405.

[4] M. Nesterova and S. Nicol, Analytical Study of 5G Beamforming in the Reactive Near-Field Zone, EuCAP Conference, London, April 2018.